Proceedings of the
47th IEEE Conference on Decision and Control
Cancun, Mexico, Dec. 9-11, 2008

WeB18.5

Extending the RWM Stability Region by Optimal Feedback Control

J. Dalessio, E. Schuster, D. Humphreys, M. Walker, Y. In, J.S. Kim

Abstract— The stabilization of the resistive wall mode (RWM) instability in the DIII-D tokamak is necessary to maintain conditions for the plasma experiment. Stability has been achieved in experiments using proportional/derivative (PD) gain controllers. However, the stability range in terms of the mode growth rate γ is limited. Employing an optimal feedback controller in conjunction with a state estimator designed to reject sensor colored noise, the stability region of the system is greatly extended. Using experimental results, the power spectral density of the measurement noise is used to model the colored noise as a noise transfer function with a white noise input. The Linear Quadratic Gaussian (LQG) control technique is applied and results are compared to a traditional PD controller through simulations.

I. INTRODUCTION

A well known instability in the field of magnetohydrodynamic (MHD) physics is the resistive wall mode (RWM), which occurs in high-pressure plasmas in toroidal magnetic confinement fusion devices such as the tokamak ([1], [2]). The RWM is a form of plasma kink instability that deforms the entire plasma configuration symmetrically in the helical direction with an extremely fast MHD Alfvenic time scale ($\sim \mu s$). The presence of the conductive tokamak structure acts as a stabilizing mechanism through the eddy currents that are induced by the time-varying magnetic perturbations generated by the plasma deformation. These induced currents generate magnetic fields that oppose the plasma deformation, resulting in a slower growth time ($\sim ms$) of the RWM, which allows the use of feedback to control this mode [3]. The inherent resistive losses of the surrounding structure cause a decay in the induced wall currents reducing the stabilizing effect of the wall. Current research focuses on the stabilization of the first ($n = 1$) kink mode (the plasma perturbation repeats only once as the toroidal angle varies from 0 to 2π) since this is usually the first to occur when pressure increases.

Convention in the fusion community uses a normalized pressure coefficient β_N to measure the efficiency of confinement of the plasma. The range of interest for the control of the RWM is between the critical β_N value where the plasma becomes unstable without a perfectly conducting wall and the critical β_N where the RWM is unstable even with

the perfectly conducting wall due to high plasma pressure. This is the range between the "no-wall beta limit" $\beta_{N,no-wall}$ and the "ideal-wall beta limit" $\beta_{N,ideal-wall}$. The normalized plasma pressure efficiency β_N is further normalized based on the limits of interest to form a new variable $C_\beta = \frac{\beta_N - \beta_{N,no-wall}}{\beta_{N,ideal-wall} - \beta_{N,no-wall}}$, where C_β is a measure of the stability of the plasma to resistive wall modes. For $C_\beta < 0$ the RWM is always stable and for $C_\beta > 1$ the plasma cannot be practically stabilized. The range of interest for control of the RWM is $0 < C_\beta < 1$. Further, there exists a relationship between the normalized measure of stability C_β and growth rate of the RWM γ. There are efforts to fully understand this relationship, yet typically the growth rate increases for increasing C_β [4].

There have been many successful efforts on feedback stabilization of resistive wall modes in DIII-D [5], [6] as well as other toroidal experiments, such as HBT-EP [7] and NSTX [8]. Most of the stabilizing efforts in this field focused on designing non-model-based, empirically-tuned controllers with *PD* (proportional-derivative) action, without taking advantage of developed models. One problem with PD controllers used in present experiments is that they require substantial derivative gain for stabilization, which implies a large response to noise, leading to a requirement for high peak voltages and coil currents. Linear Quadratic Gaussian (LQG) controllers show the potential of overcoming this limitation by making use of Kalman filters to smooth estimates of the unstable mode and by exploiting the a-priori knowledge (model) of the system. There have been some efforts on developing LQG optimal controllers based on state-space representations of circuit models for the DIII-D tokamak [9] and ITER [10]. Although these previous controllers have been proved effective through simulation in extending the stability region of the closed-loop system, they do not exploit experimental results to model the color of the measurement noise.

This work uses the General Atomics (GA)/Far-Tech DIII-D RWM model, which exhibits more detail and complexity than those models considered in previous work for DIII-D. The model replaces the perturbed plasma surface by a perturbed toroidal current sheet, and models the resistive wall using an eigenmode approach [11], [12]. The plasma surface and current sheet perturbations are equivalent in the sense that they both produce the same magnetic field perturbation. Using Faraday's Law, a set of inductive circuit equations form the state space model that embeds a scalar coupling coefficient c_{pp}, which is inversely related to the growth rate γ of the mode. Although the plasma surface deformation cannot
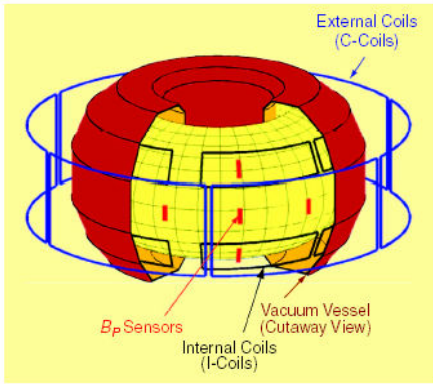
Fig. 1. Coils and sensors for RWM magnetic feedback stabilization.

Fig. 2. Empirical relationship between the growth rate γ and c_{pp}.

be directly measured in real time, the magnitude and phase of the deformation can be diagnosed from measurements by a set of 22 magnetic field sensors composed of poloidal magnetic field probes and saddle loops, which measure radial flux. A set of 12 internal feedback control coils (I-coils) can then be used to return the plasma to its original axisymmetric shape. Fig. 1 shows the arrangement of coils and sensors. Using an estimator for the two orthogonal components of the assumed $n = 1$ mode pattern, the 22 outputs are reduced to 2 outputs that represent the sine and cosine components of the RWM. These two outputs can be combined to express the output as a signal composed of the RWM amplitude and toroidal phase [13]. The quartet configuration for the I-coils reduces the number of controllable inputs by locking the phase of the I-coils in sets of four, 120 degrees apart. Thus, the original 12 inputs are reduced to 3 inputs, which represent three I-coil circuits that are independently controllable by the quartet configurations.

The overall goal of this work is to use the developed DIII-D RWM model to design a model-based optimal feedback controller for RWM stabilization over a predefined range of the growth rate γ, extending the theoretical stability range to the ideal wall limit ($C_\beta = 100\%$). The color of the measurement noise is modeled by taking advantage of experimental data, and an augmented plant model is used for controller design. The paper is organized as follows. Section II introduces the GA/Far-Tech DIII-D RWM plasma model. Section III describes the design of the optimal feedback controllers using the LQG control technique. Section IV describes the manipulation of experimental data to model the colored measurement noise and augment the plasma model. In Section V, the performance of this controller is assessed through simulations. Section VI closes the paper by stating the conclusions.

II. PLASMA MODEL

A. System Model

The matrices in the model represent characteristics of the tokamak and are well known. The uncertainty is introduced through the variable c_{pp}, which corresponds to a certain growth rate γ of the resistive wall mode. The relationship between these variables is shown in Fig. 2 for a particular plasma equilibrium and is further explained in [12].
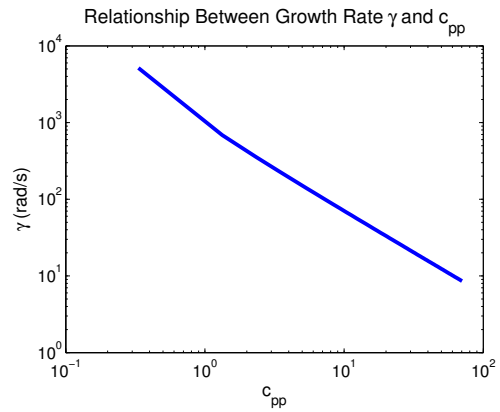
The model is represented in terms of the couplings between the plasma (p), vessel wall (w), and coils (c). The model derived from Faradays law of induction results in the system dynamics that reduce to

$$(M_{ss} - M_{sp}c_{pp}M_{ps})\dot{I}_s + R_{ss}I_s = V_s \quad (1)$$

where M_{ss} is the mutual inductance between external conductors, including the vessel wall and the coils, M_{sp} is the mutual inductance between external conductors and the plasma, R_{ss} is the resistance matrix, I_s is the current flowing in the conductors, and V_s is the externally applied voltage to the conductors. The mutual inductance matrices are given by

$$M_{ss} = \begin{bmatrix} M_{ww} & M_{wc} \\ M_{cw} & M_{cc} \end{bmatrix}, M_{sp} = \begin{bmatrix} M_{wp} \\ M_{cp} \end{bmatrix}, M_{ps} = \begin{bmatrix} M_{pw} & M_{pc} \end{bmatrix},$$

where M_{ps} and M_{sp} satisfy the following condition

$$M_{ps} = M_{sp}^T = \begin{bmatrix} M_{wp}^T & M_{cp}^T \end{bmatrix} \Rightarrow M_{pw} = M_{wp}^T, M_{pc} = M_{cp}^T.$$

The resistance matrix is given by

$$R_{ss} = \begin{bmatrix} \lambda_w & 0 \\ 0 & R_c \end{bmatrix},$$

where λ_w characterizes the couplings of a wall surface eigenmode to other states by the time-varying perpendicular magnetic fields contributed by those states and R_c is the coil resistance. The current and externally applied voltage to the conductors can be written as

$$I_s = \begin{bmatrix} I_w \\ I_c \end{bmatrix}, V_s = \begin{bmatrix} 0 \\ V_c \end{bmatrix},$$

where I_w is the wall current, I_c is the coil current, and V_c is the externally applied voltage to the coil.

This model can be represented in a state space formulation using the current in the conductors as the states ($x = I_s$) and the applied voltage as the inputs ($u = V_s$). This results in the following state space equation

$$\dot{x} = Ax + Bu \quad (2)$$

where $A = -L_{ss}^{-1}R_{ss}$, and $B = L_{ss}^{-1}$, with $L_{ss} = M_{ss} - M_{sp}c_{pp}M_{ps}$. The output equation of the state space representation is based on sensor measurements that relate to the conductor currents through the dynamics

$$y = Cx \quad (3)$$

where $C = C_{ss} - C_{yp}c_{pp}M_{ps}$, C_{yp} is the coupling matrix between the sensor and plasma current, and $C_{ss} = \begin{bmatrix} C_{yw} & C_{yc} \end{bmatrix}$ is given by the coupling matrix between the sensor and wall current C_{yw}, and the coupling matrix between the sensor and coil current C_{yc}.

B. Noise Effect Model

The operation of DIII-D introduces both process noise to the systems states and measurement noise to the system outputs. The state space system model is therefore modified to include the noise effect,

$$\dot{x} = Ax + Bu + Gw_1, \tag{4}$$
$$y = Cx + v, \tag{5}$$

where w_1 is the process noise and v is the measurement noise. The process noise scaling matrix is assumed as $G = I_n$, where I_n denotes the $n \times n$ identity matrix and n is the number of states. The noise w_1 is assumed to be zero-mean, white noise with covariance given by $Q = E(w_1 w_1^T)$, where E denotes the expectation operator. The measurement noise is characterized by the covariance matrix $R = E(vv^T)$. Experimental data suggests that the measurement noise in DIII-D is not white, having a particular frequency content. The measurement noise v is then modeled as a zero-mean, colored noise.

III. LQG OPTIMAL FEEDBACK CONTROLLER

With the ultimate goal of minimizing both the total fluctuation energy of the instability and the control power, we make use of the LQG optimal control theory. By exploiting the separation principle, the LQG controller combines a linear quadratic regulator (LQR) (state feedback controller) and a Kalman filter (state estimator).

The state feedback law $u = -Kx$, where K is the state feedback gain matrix, is obtained by minimizing the quadratic cost function,

$$J(u) = \int_0^\infty \left(x^T Q_w x + u^T R_w u \right) dt \tag{6}$$

where Q_w (at least positive semi-definite) and R_w (positive definite) are weighting matrices for the states and inputs respectively. The state feedback gain of the *LQG* controller is given by

$$K = R_w^{-1} B^T S, \tag{7}$$

where S is the solution of the associated Riccati equation

$$A^T S + SA - SBR_w^{-1} B^T S + Q_w = 0. \tag{8}$$

The state estimation $\hat{x}$ is provided by the Kalman filter

$$\dot{\hat{x}} = A\hat{x} + Bu + L(y - C\hat{x}) \tag{9}$$

where L is the Kalman gain matrix obtained by minimizing the trace of the estimation error $x(t) - \hat{x}(t)$ covariance under the assumption that both the process noise and the measurement noise are zero-mean and white (constant power spectral density). The gain of the state estimator is given by

$$L = PC^T R^{-1}, \tag{10}$$

where P is the solution of the algebraic Riccati equation,

$$0 = AP + PA^T + BQB^T - PC^T R^{-1} CP, \tag{11}$$

with Q and R denoting the process and sensor noise covariance matrices.

The final controller is governed by the state-space equations

$$K_{LQG} : \begin{cases} \dot{\hat{x}} = [A - LC - BK]\hat{x} + Ly \\ u = -K\hat{x} \end{cases} \tag{12}$$

IV. MODELING OF COLORED NOISE

The energy of the time domain signal $u(t)$, which is the energy per unit time (instantaneous power $u^2(t)$) integrated over all time, can be expressed using Parseval's relation as the energy per unit frequency integrated over all frequency

$$E = \int_{-\infty}^\infty u^2(t)dt = \frac{1}{2\pi} \int_{-\infty}^\infty F^*(\omega)F(\omega)d\omega \triangleq \int_{-\infty}^\infty \Psi(\omega)d\omega \tag{13}$$

where $F(\omega)$ denotes the Fourier transform of $u(t)$, and $\Psi(\omega) = \left| \frac{1}{\sqrt{2\pi}} \int_{-\infty}^\infty u(t)e^{-j\omega t}dt \right|^2 = \frac{|F(\omega)|^2}{2\pi}$ is the energy spectral density, which describes how the energy (or variance) E of a time signal is distributed with frequency [14].

Stochastic signals are not absolutely integrable or square integrable, and consequently do not have Fourier transforms. In this case, the concept of energy spectral density is not useful. However, many of the properties of stationary stochastic processes, where the statistical properties are invariant to a shift of time origin, can be summarized in terms of the auto-covariance function, for which the Fourier transform often exists. As an alternative to the energy spectral density, we use the power spectrum density (PSD) $\Phi_{uu}(\omega)$, which describes how the power P of a time signal is distributed with frequency and is the Fourier transform of the auto-covariance sequence $C_{uu}(\tau) = E\{u(t)u(t - \tau)\}$,

$$\Phi_{uu}(\omega) = \int_{-\infty}^\infty C_{uu}(\tau)e^{-j\omega\tau}d\tau, \quad P = \int_{-\infty}^\infty \Phi_{uu}(\omega)d\omega \tag{14}$$

where we assume without loss of generality that $E\{u(t)\} = 0$.

For a linear time-invariant (LTI) system with impulse response $h(t)$, the output sequence $y(t)$ is related to the input sequence $u(t)$ through the convolution integral,

$$y(t) = h(t) * u(t) \triangleq \int_{-\infty}^\infty h(t)u(t - \tau)d\tau, \tag{15}$$

and the relationship for the input and output PSD's is given by

$$\Phi_{yy}(\omega) = |H(j\omega)|^2 \Phi_{uu}(\omega), \tag{16}$$

where $H(s)$ is the Laplace transform of the impulse response $h(t)$ (transfer function of the system).

In order to model the color of the measurement noise present in the DIII-D, we are interested in finding a transfer function $H_v(s)$ that will produce an output v with the same PSD observed from experimental data, when we have a zero-mean, unitary-variance, white noise w_2 at the input, i.e., $v(s) = H_v(s)w_2(s)$. Since $\Phi_{w_2 w_2}(\omega) = 1$ by definition of white noise, using (16) we obtain that

$$\Phi_{vv} = |H_v(j\omega)|^2. \tag{17}$$
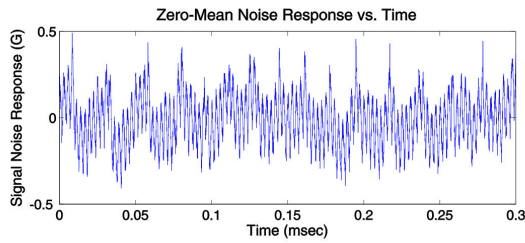
Fig. 3. Typical sensor noise signal in DIII-D.
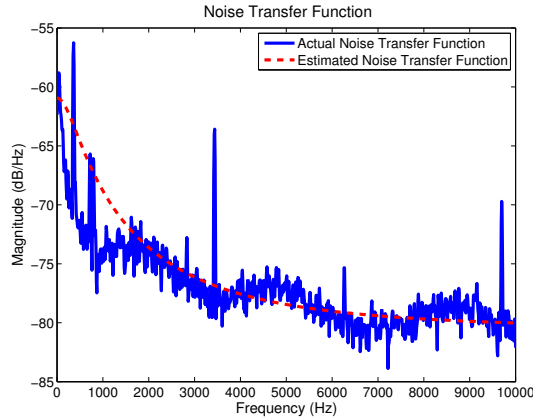
Fig. 4. Computed and estimated noise transfer function.

Fig. 3 shows a typical zero-mean measurement noise signal in one of the 22 diagnostics used for RWM control in DIII-D. Using (17) we can conclude that $|H_v(j\omega)| = \sqrt{\Phi_{vv}(\omega)}$. Fig. 4 shows the square root of the computed PSD $\Phi_{vv}(\omega)$ for the noise signal (solid blue line). Using the Matlab fitting algorithm "fitmagfrd," we obtain an estimate for the noise transfer function $H_v(s)$, which is also shown in Fig. 4 (dashed red line).

This procedure can be carried out for each of the 22 sensors. Each transfer function can be written in state space representation as

$$\dot{x}_v = A_v x_v + B_v w_2 \qquad (18)$$

$$v = C_v x_v + D_v w_2. \qquad (19)$$

Finally the modeled color noise can be augmented with the original system to form

$$\tilde{x} = \begin{bmatrix} x \\ x_v \end{bmatrix}, w = \begin{bmatrix} w_1 \\ w_2 \end{bmatrix} \qquad (20)$$

$$\dot{\tilde{x}} = \begin{bmatrix} A & 0 \\ 0 & A_v \end{bmatrix} \tilde{x} + Bu + \begin{bmatrix} G & 0 \\ 0 & B_v \end{bmatrix} w \qquad (21)$$

$$y = \begin{bmatrix} C & C_v \end{bmatrix} \tilde{x} + \begin{bmatrix} 0 & D_v \end{bmatrix} w. \qquad (22)$$

V. CONTROLLER SYNTHESIS AND SIMULATION

A. Controller and Kalman Filter Synthesis

The LQG controller synthesis is applied to both systems considered, model (4)-(5) without the model for the colored noise and model (21)-(22) with the model for the colored noise. By doing this we intend to quantify the effect of neglecting the color of the noise during the Kalman filter design. The choice of the weighting parameters is made such

that slightly more weight is placed on the system inputs and less on the states. This is achieved with Q_w and R_w weighting matrices that are diagonal matrices of 1.0×10^{-2} and 1.0 respectively. These design parameters increase the damping and decrease the bandwidth, which decreases the response time of the controller [15]. However, the controller design can still perform to the design constraints.

For the base case where the color of the measurement noise is neglected (i.e., the measurement noise v is erroneously assumed white during the Kalman filter design), the Q and R covariance matrices are given by 1.0×10^4 and 1.0×10^{-11} respectively. This design choice helps to decrease process noise and increase reliance on sensor noise, which effectively results in a fast estimation response. For the case where the color of the measurement noise is modeled, the measurement noise is included in the process noise causing an augmented Q matrix. The process noise part of the covariance matrix Q remains 1.0×10^4, while the modeled measurement noise part of the Q matrix has a covariance of 3.5×10^3. The covariance matrix R is now set to zero.

The complete system that is used to design the controller has an additional two time delay blocks preceding the plasma model. The time delays physically represent the plasma control system and the power supply. For design purposes, the time delays are linearized using second order Padé approximations.

These controllers were designed using a c_{pp} value of 0.29 ($\gamma = 6,900$) using the 29 eigenmode model with 64 states. The base case controller was designed with an order of 73, but using model reduction the order was reduce to 8 while maintaining similar performance characteristics. The controller with the modeled colored noise was designed with an order of 139, but was also reduced to 8 with minimal performance effects.

B. Controller Simulation and Results

In order to be able to compare the proposed model-based *LQG* controllers with present non-model-based controllers, a proportional-derivative (*PD*) controller is designed (integral action is not required for this system). The *PD* controller is synthesized to maximize the stability range as a function of γ and is of the form

$$K_{ij} = \frac{G_{P_{ij}} + G_{D_{ij}} s}{1 + \tau_{pcs} s} \qquad (23)$$

where i is the index for the control inputs into the system ($i = 1 \ldots 3$), j is the index for the number system outputs ($j = 1 \ldots 2$), $G_{P_{ij}}$ is the proportional gain, $G_{D_{ij}}$ is the derivative gain, and τ_{pcs} is the time constant taken to be 4×10^{-4} sec. Each K_{ij} term fills the 3×2 controller matrix K. It was found that the stability range can be maximized by a controller with non-zero K_{11}, K_{22}, and K_{32} terms and every other term set to zero. Using *PD* controllers for the terms K_{11}, K_{22}, and K_{32}, all six gains are optimized to obtain the maximum range of stability as a function of γ. The resulting gains are

TABLE I
PERFORMANCE TARGETS AND CONSTRAINTS.

Condition	Target Value	Maximum Constraint
Rise Time	1.0ms	5.0ms
Settling Time	5.0ms	10ms
Input Voltage	N/A	$\pm$ 100V
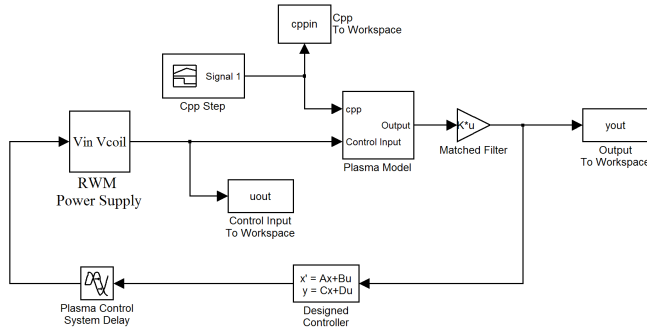
Fig. 5.   Top Level of the Simulink model.

$$G_{P_{11}} = 3.80 \times 10^4 \qquad G_{D_{11}} = 76$$
$$G_{P_{22}} = 1.38 \times 10^4 \qquad G_{D_{22}} = 40$$
$$G_{P_{32}} = 6.62 \times 10^4 \qquad G_{D_{32}} = 103.$$

The performance of the LQG controllers are simulated using a Simulink model of the plasma, controller, plasma control system, and power supply and compared to the results of a well-tuned *PD* controller. The top level of the Simulink model is presented in Figure 5. The power supply has a saturation block that realizes the physical limit of the applied voltage of ± 100 V. The applied process noise is a white noise element while the sensor noise is the modeled colored noise with covariance defined by the controller design values. Table I provides the performance constraints in response to a unit step in the RWM mode amplitude.

Fig. 6 shows the time response to initial conditions of the plasma, normalized to a starting RWM mode amplitude of 1 Gauss. This simulation is performed at constant RWM growth rates of $\gamma = 10$ rad/s and $\gamma = 5,000$ rad/s, the lower and upper limits of the growth rate range of our interest. In both cases, the *LQG* controllers provide quick suppression of the RWM mode amplitude, out-performing the *PD* controller, which does not provide quick suppression at the faster growth rate and even shows a longer settling time for the slower growth rate.

Another example is presented in Fig. 7, which shows the time response to a unit step disturbance in the RWM mode amplitude. Once again, the simulation is performed with constant growth rates, which define our range of interest. For the slower growth rate (top graph), all three controllers have a similar rise time, minimal overshoot, and settling time. For the faster growth rate, the settling time for all the controllers is increased. The PD controller converges to a bigger steady-state offset when compared to the LQG controllers.
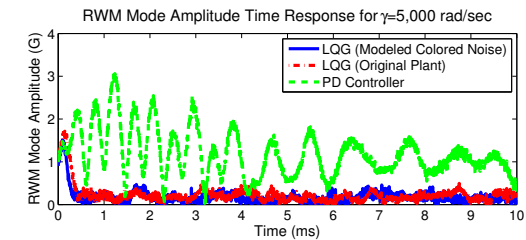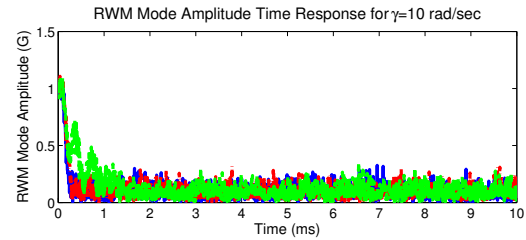
Fig. 6.   Initial condition response RWM mode amplitude for $\gamma = 10$ rad/s (top) and $\gamma = 5,000$ rad/s (bottom).
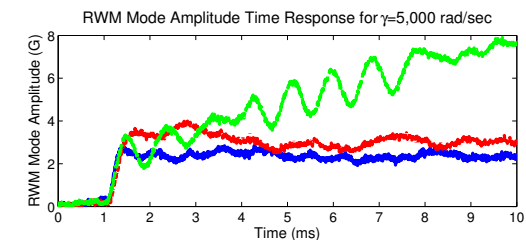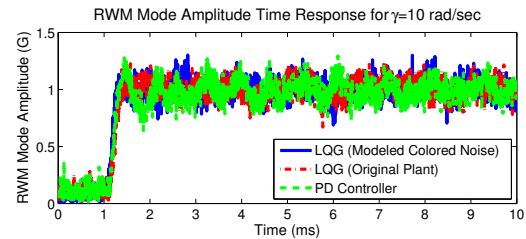
Fig. 7.   Step response RWM mode amplitude for $\gamma = 10$ rad/s (top) and $\gamma = 5,000$ rad/s (bottom).

C. Closed-loop Stability and Performance

It is useful to determine the range of γ where the system remains stable as well as the range where the system performs within the limits of the performance constraints (see Table I). Table II provides the ranges of γ for which stability and performance conditions are satisfied. The first row (*Stability Range*) indicates the range of γ for which the system remains stable when using a unit step disturbance for the RWM model amplitude. The second row (*Perf. Range (Initial)*) indicates the range of γ for which the performance conditions are satisfied when an initial unit excitation of the RWM mode amplitude is forced through appropriate initial conditions. Both model-based *LQG* controllers show good stability and performance properties well beyond the desired γ range and that of the *PD* controller, with the *LQG* controller design that exploits the model of the colored noise having a larger range in both stability and performance.

As a final check of the controllers' performance, the measurement noise characteristics are determined. A test is performed to find the RMS noise level of the RWM mode

TABLE II
γ STABILITY AND PERFORMANCE RANGES.

Controller	LQG	LQG w/ Noise	PD
Stability	0 - 7,300 rad/s	0 - 9,000 rad/s	0 - 3,800 rad/s
Perf. (Initial)	0 - 5,800 rad/s	0 - 7,300 rad/s	0 - 3,800 rad/s
RMS Noise	4.50 G	4.50 G	0.75 G
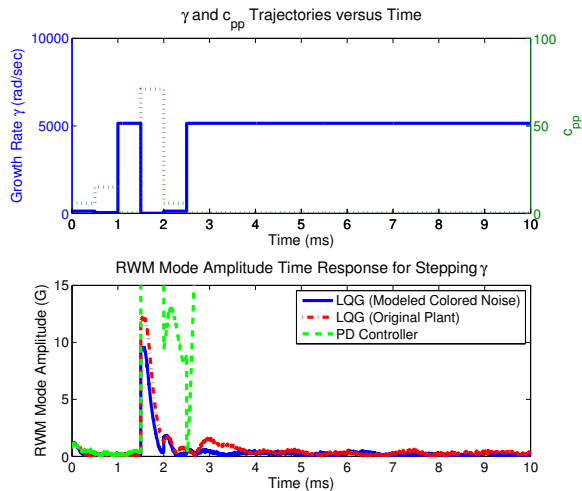
Fig. 8.   Initial condition response control inputs for stepping γ.

amplitude that can be sustained until instability is reached due to the input voltage constraints. The third row in Table II summarizes the approximate RWM mode amplitude noise level at which this occurs. The row *RMS Noise* corresponds to an initial condition response test at a growth rate of $\gamma = 5,000$ rad/s to determine the maximum noise level before instability was reached. Both *LQG* controllers can withstand large amounts of sensor noise compared to the *PD* controller.

Since the optimal feedback controllers stabilize the plant over a range of growth rate, it is of interest to investigate the controller performance using time-varying of growth rate γ. The results for a stepping and sinusoidal excitation of the c_{pp} parameter are presented (Fig. 8-9). The step function also
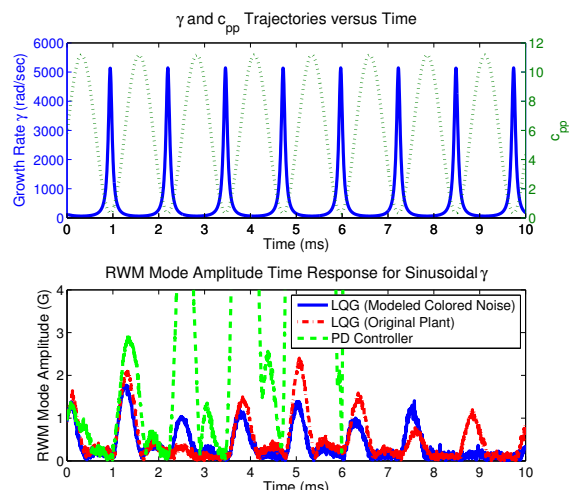
Fig. 9.   Initial condition response control inputs for sinusoidal c_{pp}.

initiates at $c_{pp} = 5.75$ and changes between the maximum, nominal, and minimum values of c_{pp} in 0.5 ms intervals over a 2.5 ms span. The amplitude of the sinusoidal function in c_{pp} is 5.4175 with an offset of the nominal value ($c_{pp} = 5.75$), which results in a function reaches the highest growth rate in the design range. Its frequency is 5,000 rad/sec. In both cases the RWM mode amplitude is quickly suppressed (Fig. 8-9). The *LQG* controller including the colored noise model maintains less RWM amplitude compared to the base case *LQG* controller, providing better rejection to changes in the growth rate. In all cases the *PD* controller has difficulty suppressing the RWM amplitude and becomes unstable.

VI. CONCLUSIONS

A colored noise transfer function was deduced using the power spectral density of experimental data and estimating a model with a white noise input. The stabilization region of the RWM was successfully extended by applying an optimal feedback control law and state estimator (LQG) to the augmented state space model using colored noise. The stability region was significantly improved with the model-based control as opposed to the non-model-based, empirically-tuned PD controller, while maintaining a controller order that can be implemented.

REFERENCES

[1] J. Wesson,*Tokamaks*, Clarendon Press, Oxford, 3rd ed., 2004.
[2] A. Pironti and M.L. Walker,"Fusion, Tokamaks, and Plasma Control," *IEEE Control Systems Magazine*, v 25, n 5, October 2005, p.30-43.
[3] Walker M.L., Humphreys D.A. *et al.*, "Emerging Applications in Tokamak Plasma Control," *IEEE Control Systems Magazine*, v 26, n 2, April 2006, p.35-61.
[4] Strait E.J., Bialek J. *et al.*, "Resistive wall stabilization of high-beta plasmas in DIII-D," *Nucl. Fusion* **43**, 2003, p.434.
[5] Garafalo A.M., *et al*, "Resistive wall mode dynamics and active feedback control in DIII-D," *Nucl. Fusion*, v 41, n 9, September 2001, p 1171.
[6] Okabayashi M., *et al*, "Control of the resistive wall mode with internal coils in the DIII-D tokamak," *Nucl. Fusion*, v 45, n 12, December 2005, p 1715-31.
[7] S. Mauel *et al*, "Dynamics and control of resistive wall modes with magnetic feedback control coils: experiment and theory," *Nuclear Fusion*, v 45, n 4, April 2005, 285-93.
[8] S. Sabbagh *et al*, "The resistive wall mode and feedback control physics design in NSTX," *Nuclear Fusion*, v 44, n 4, April, 2004, p 560-570.
[9] Sen A.K., *et al*, "Optimal control of tokamak resistive wall modes in the presence of noise," *Phys. Plasmas*, v 10, n 11, November 2003, p 4350.
[10] Katsuro-Hopkins O., *et al*, "Enhanced ITER resistive wall mode feedback performance using optimal control techniques," *Nucl. Fusion*, v 47, n 9, Sep 1, 2007, p 1157-1165.
[11] C.M. Fransson, D. H. Edgell, D. A. Humphreys and M. L. Walker, "Model validation, dynamic edge localized mode discrimination, and high confidence resistive wall mode control in DIII-D," *Phys. Plasmas*, v 10, n 10, October 2003, p 3961.
[12] Y. In, *et al*,"Model-based dynamic resistive wall mode identification and feedback control in the DIII-D tokamak," *Phys. Plasmas*, v 13, n 6, June 2006, p 62512-1-12.
[13] Edgell D.H., Kim J.S. *et al.*, "Magnetohydrodynamic mode identification from magnetic probe signals via a matched filter method," *Rev. Sci. Instrum.*, v 73, n 4, April 2002, p 1761.
[14] Oppenheim A. and Willsky A. *Signals and Systems*, Prentice-Hall, 1997.
[15] Franklin G. F. and Powell J. D., *Digital Control of Dynamic Systems: 3rd Edition*. Addison Wesley Longman, Inc., Menlo Park, CA, 1998. pg. 44.